Pathological α-Synuclein Perturbs Nuclear Integrity

Michael Millett[1], Allison Comite[1], Elisabeth Martin Castosa[1], Anika Heuberger[1], Preston Wagner[1], Ignacio Gallardo[1], Jessica Reinhardt[1], Nicole Chambers[1], Dominic Hall[1], Evan Miller[1], Douglas Nabert[1], Barbara Balsamo[1], Stefan Prokop[2], Mark Moehle[1&2]

[1]Department of Pharmacology & Therapeutics and Center for Translational Research in Neurodegeneration, University of Florida College of Medicine, Gainesville, FL 32610

[2]Department of Pathology, Norman Fixel Institute for Neurological Diseases and Center for Translational Research in Neurodegeneration, University of Florida College of Medicine, Gainesville, FL 32610

[&]To Whom Correspondence Should Be Addressed:
Mark S. Moehle, PhD
1200 Newell Drive
ARB R5-252
Gainesville, FL 32610
mark.moehle@ufl.edu

Abstract:
Pathological aggregates of α-synuclein are a hallmark of a group of neurodegenerative disorders collectively termed synucleinopathies. The physiological function of α-synuclein and the detrimental effects of the pathological variants of α-synuclein have been widely debated, but recent evidence has suggested an emerging consensus on a critical role for α-synuclein in regulating synaptic function. However, a controversial role for α-synuclein in nuclear function in both normal and pathogenic states has been proposed, and the degree to which α-synuclein localizes within the nucleus and subsequent impact on the nucleus are poorly understood. To begin to address this controversy, we employed synucleinopathy murine and cell culture models, as well as postmortem human Lewy Body Dementia tissue to elucidate the extent to which pathological α-synuclein localizes within the nuclear compartments, and the downstream consequences of this localization. We observed pathological aggregation of α-synuclein within the nucleus in both murine models and human postmortem Lewy Body Dementia cortex via quantitative super resolution microscopy. In both mouse and human brain tissue the presence of α-synuclein in the nucleus correlated with abnormal morphology of nuclei. This pathological accumulation of α-synuclein in the nucleus was not observed in control mice, human tissue without pathology, or control cells. We subsequently examined the mechanistic consequences of pathological accumulation of α-synuclein in the nucleus. Synucleinopathy models displayed increased levels of the DNA damage marker 53BP1. Furthermore, cells with pathological α-synuclein exhibited elevated markers of nuclear envelope damage and abnormal expression of nuclear envelope repair markers. Our cell culture data also suggests altered RNA localization in response to pathological α-synuclein accumulation within the nucleus. Lastly, we show that nuclear Lewy-like pathology leads to increased sensitivity to nuclear targeted toxins. Taken together, these results rigorously illustrate nuclear localization of pathological α-synuclein with super resolution methodology and provide novel insight into the ensuing impact on nuclear integrity and function.

Introduction:

Alpha-synuclein (α-syn) is a small, 140 amino acid protein, that is predominantly expressed in neurons, compromising up to 1% of the total protein content of the brain (Maroteaux et al., 1988). Pathological α-syn (p-α-syn) is a hallmark feature of a group of neurodegenerative diseases, termed synucleinopathies, in which α-syn accumulates into hyperphosphorylated, ubiquitinated, insoluble, and high molecular weight aggregates. Pathological α-syn aggregates are found throughout multiple cell types and brain regions across synucleinopathies. α-syn was initially identified in the electric lobe of the *Torpedo californica*, and was found to have expression spanning from the presynaptic terminal to within the nucleus (Maroteaux et al., 1988; M. S. Nielsen et al., 2001). In decades of research since its initial discovery, α-syn has been shown to have a critical role in synaptic function such as neurotransmitter release and regulation of synaptic vesicle dynamics in mammals in both pathological states and normal physiology (Burré, 2015; Jo et al., 2000; Man et al., 2021; Snead & Eliezer, 2014). However, a role for α-syn in nuclear function has remained controversial.

There are a number of reports of both homeostatic and pathogenic α-syn variants having nuclear localization and function in models of synucleinopathies (McLean et al., 2000; Mori et al., 2002; Schaser et al., 2019). Recent studies have indicated that α-syn may directly bind DNA, and have a role in DNA damage repair (Schaser et al., 2019). Overexpression of α-syn within the nucleus is strongly correlated with nuclear stress, nuclear dysfunction, altered behavioral outcomes, and increased neurodegeneration (T. Du et al., 2024; Pan et al., 2023). However, studies that rely on over-expression of α-syn are obscured by the fact that small proteins less than 40 kDa can passively diffuse into the nucleus (Jamali et al., 2011).Furthermore, pathogenic *SCNA* mutations have been shown to impact nuclear envelope integrity and function (Chen et al., 2020). Additionally, in postmortem studies of human tissue, both normal and pathological α-syn, termed Lewy pathology (Lewy, 1912), have been suggested within the nucleus via immunofluorescence microscopy and biochemical assays (Koss et al., 2022). Despite this body of evidence, the function or localization of α-syn in the nucleus has remained controversial due to insufficient resolution to definitively determine localization, and a number of initial reports being confounded by off target binding of initial α-syn antibodies in the nucleus (Huang et al., 2011; Koss et al., 2022).

Here, we address the nuclear localization of p-α-syn utilizing the pre-formed fibril (PFF) model of α-synucleinopathies in rodents and cell culture. We characterize the extent pathological α-syn localizes to the nucleus via quantitative super-resolution microscopy. Additionally, we elucidate the effects of nuclear localization on envelope integrity, nucleic acid damage, and function of the nucleus with biochemical and cell-based analysis. Our results identify nuclear envelope abnormalities, DNA damage, increased susceptibility to nuclear insult, and potential deficits in envelope repair resulting from the nuclear and peri-nuclear localization of pathological α-syn. Nuclear p-α-syn and aberrant nuclear morphology was confirmed with postmortem human tissue. Our data provides additional insight into nuclear α-syn in the context of synucleinopathies and suggests new mechanisms to the etiology of these neurodegenerative disorders.

Results:

Synucleinopathy Mice Display Robust Cortical Lewy-like Pathology

To characterize the morphology of pathological α-syn aggregates in murine brain tissue we employed an antibody specific to p-α-syn phosphorylated on Serine 129 (Abcam EP1563Y), an established biomarker for p-α-syn (Anderson et al., 2006; Fujiwara et al., 2002; Okochi et al., 2000; Parra-Rivas et al., 2023). All reagents and materials for tissue immunofluorescence can be found in Table 1. Abundant p-α-syn signal was observed in the mouse cortex, specifically deep cortical layers (Fig 1A). Super resolution imaging of PFF-injected cortical neurons revealed complex ultrastructural shapes of Lewy-like pathology. Analysis of these images revealed six characteristic nuclear or perinuclear morphologies of p-α-syn in the cortex (Fig 1B). Examining the presence of nuclear interacting p-α-syn over time revealed a dynamic change in interaction with the nucleus. Using micrographs acquired both at 6-weeks and 6-months post PFF injection we found differential distribution of nuclear or perinuclear morphology. These data show p-α-syn aggregation is a dynamic process with significantly more punctate and neuritic pathology at 6 weeks and more fibril-like pathology at 6-months post PFF injection ($p<0.0001$, Fisher's Exact Test) (Fig 1C).

Pathological α-Syn Localizes Within Nuclear Compartments.

Next, to determine if pathological aggregates of α-syn localize within the nucleus, we examined p-α-syn fluorescent signal localization within Lamin A/C (Abcam) structures for quantification. Lamin A/C was chosen as an internal "cutoff" structure to qualify if p-α-syn localizes within the nuclear compartments as it lines the inner most portion of the nuclear envelope (Fig. 2B, Left) (Aebi et al., 1986). Using IMARIS software (Oxford Instruments) we generated 3D surface renderings based off of absolute fluorescent intensity to aid in quantification and visualization (Fig. 2A). Using this pipeline, we implemented a 240 μm lateral and 600 μm axial localization depth for p-α-syn within the nucleus as another "cutoff" metric for quantification to account for resolution limits of our image acquisition (Sup. Fig. 1). We found 86.7% (95% CI 70.32-94.69%) of p-α-syn aggregates had substantial nuclear localization within the Lamin A/C structure (Fig. 2B, Right). See supplemental video 1 for animation of p-α-syn aggregation within nuclear compartments.

To determine if pathological p-α-syn is present in the nucleus in human synucleinopathies, as previously suggested, (Koss et al., 2022), we processed and analyzed control and Lewy Body Dementia (LBD) tissue as described for murine tissue with minor modifications (see Materials and Methods). Human LBD Lewy Pathology was primarily neuritic with high density of small punctate, shapes, and neuritic morphology (Fig. 2C) (Sup. Fig. 2). The large cortical Lewy bodies analyzed were predominantly large aggregates of small p-α-syn inclusions, but some have fibril-like components attached to the punctate mass (Fig 2D). Both control and LBD tissue had some level of Lamina damage and/or degradation (Fig 2C) that could likely be attributed to the postmortem interval (PMI) before tissue fixation (Badonic et al., 1992; Blair et al., 2016). Due to varied levels of nuclei integrity (Sup. Fig. 3), Lamin surface renderings were only generated for visualization purposes on high integrity nuclei (Fig 2E). See supplemental video 2 for animation. Cortical Lewy Bodies are largely perinuclear but with significant levels of nuclear localization as well (Fig. 2E, 2F). Analyzing cortical Lewy Bodies for co-localization with DAPI and found nuclear localization to also be a hallmark of LBD, with 95% of these aggregates having nuclear localization (Fig 2F). Of the aggregates quantified, 60% (95% CI 38.66 to 78.12) were associated with nuclear abnormalities (Fig 2F bottom), suggesting Lewy body pathology is contributing to envelope irregularities. See supplemental video 3 for animation of Lewy body pathology interacting with DNA.

Nuclear p-α-Syn Induces Nuclear Abnormalities

We further investigated the effects of p-α-syn nuclear localization on nuclear integrity. Envelope irregularities, which were classified as multi-lobed, malformed, or ruptured. Analyzing entire 60x field of views (1x magnification lens) we found low levels of irregularities were found in control cells, with 16% (95% CI 8.337 to 28.51) falling into these categories. Significantly more nuclei in synucleinopathy tissue displayed irregularities, with 56% (95% CI 42.31 to 68.84) falling into one of the pathological morphologies ($p<0.0001$, Chi-square value 17.36, df 1) (Fig. 3A) (Fig. 3B, Bottom). Abnormalities were found to fall into one or more of three broad classifications; multi-lobed, malformed, and/or ruptured. Of the super-resolution aggregate images acquired in Fig. 2B; 66.7% (95% CI 48.78 to 80.77) of associated nuclei were classified as abnormal (Fig. 3B, Top). Atypical phenotypes were observed at roughly equal frequency to one another, with a frequency of 35% (95% CI 11.79-40.93) multi-lobed, 30% (95% CI 9.51-37.31) malformed, and 35% (95% CI 11.79-40.93) ruptured (Fig. 3B, Top).

To quantitatively assess nuclear integrity, we next quantified sphericity of nuclear lamina structures. Sphericity (ψ) is the measure of how close a given object is to a true sphere with a maximum value of 1 (Wadell, 1932). We quantified the sphericity in synucleinopathy and control murine tissue which yielded an average of $\psi=0.3550$ (95% CI 0.3414-0.3687) and $\psi=0.5836$ (95% CI 0.5678-0.5994) respectively (Fig 3B, Bottom). Nuclei with p-α-syn show a significant decrease in nuclear sphericity ($p<0.0001$, Unpaired-T test, $t=21.60$). This suggests loss of nuclear integrity in synucleinopathy tissue spans throughout the cortex and not localized to cells with inclusions.

Synucleinopathy Models have Increased Genotoxicity

We predict loss of nuclear integrity in cortical synucleinopathy tissue was associated with increased genotoxicity as there are reports of increase DNA damage and genotoxicity in synucleinopathy models of other brain regions (Milanese et al., 2018; Szegö et al., 2022). Murine issue was probed with genotoxic and DNA

damage marker tumor suppressor P53-binding protein 1 (53BP1). 53BP1is associated with physical squeezing and damage to the nuclear envelope (Isermann & Lammerding, 2017; Shah et al., 2021), which may result from p-α-syn aggregate interaction with the nucleus. An increase in nuclear 53BP1 puncta was seen throughout the cortex, both in cells with and without p-α-syn pathology (Fig 4A left). Quantitation of nuclear 53BP1 levels revealed significantly more ($p<0.0001$, Unpaired-T test, $t=5.215$) 53BP1 puncta in synucleinopathy tissue, with an average of 66.89 puncta per cell (95% CI 54.89-78.89) while control cortical cells averaged 29.64 (95% CI 22.10-37.18) 53BP1 puncta per cell (Fig 4A, Right).

Next, we employed a cellular model of nuclear p-α-syn accumulation in synucleinopathies to define the downstream effects of nuclear localization on the cell nucleus. Adapting upon previous cell models (Sang et al., 2021), we used protein transfection of PFF's in murine Neuro 2a cells, which resulted in the robust accumulation of small p-α-syn punctate aggregates in the nucleus of the cell (Fig 4B) (Sup. Fig. 4), resembling Type V pathology in murine tissue (Fig 1B) and human Lewy Pathology (Fig 2C). See supplemental video 4 for animation of Neuro 2a nuclei with pathology. Nearly all Neuro 2a cells in culture display nuclear pathology (Sup. Fig. 4), enabling population assays. Consistent with our immunofluorescence results, western blot analysis of Neuro 2a cells for 53BP1 showed synucleinopathy cells have an 1.409x (95% CI 1.146- 1.673) increase in 53BP1 puncta compared to control cells (Fig 4B, Bottom) ($p=0.0026$, Unpaired-T test, $t=6.678$).

Pathological α-Syn Accumulation Results in Nuclear Deficits

To determine the functional impact of p-α-syn nuclear accumulation on the nucleus, we examined multiple measures of nuclear function. First, we probed RNA localization, as impaired nucleo-cytoplasmic export has been suggested synucleinopathies and other related neurodegenerative disorders (Chen et al., 2020; Woerner et al., 2016). Analysis of RNA volume renderings, from labeling with an RNA specific dye ,showed a nuclear to cytoplasmic ratio of 0.4954 (95% CI 0.3508-0.5679) for synucleinopathy tissue, and 0.09499 (95% CI0.02112-0.1689) for control tissue, demonstrating a significant decrease of RNA outside the nuclei of synucleinopathy cells (Fig. 5A) ($p=0.0003$, Unpaired-T test, $t =11.94$). This data suggests nuclear p-α-syn negatively impacts RNA export, but further studies will be necessary to determine the mechanism that results in abnormal RNA localization. Second, we investigated the impact of nuclear p-α-syn on envelope repair machinery, namely endosomal sorting complexes required for transport (ESCRT-III) repair pathway proteins (Fig 5B). Western blots were performed on synucleinopathy and control Neuro 2a cells reveals differential expression of LEMD2 and the ESCRT-III component CHMP7 (Gu et al., 2017) (Fig 5B). LEMD2, which accumulates at nuclear envelope damage/ruptures and recruits CHMP7 to initiate repair (Gu et al., 2017), displayed a 1.476x (95% CI 1.028-1.925) increase in synucleinopathy tissue ($p=0.0103$, Unpaired-T test, $t=4.568$) (Fig 5B left). Moreover, PFF treated cells expressed 0.4910x (95% CI 0.8243- 0.1578) less CHMP7 than control cells ($p=0.00028$, Unpaired-T test, $t=6.572$) (Fig 5B). Based on our results, we have generated a working hypothesis that nuclear localization of pathological α-syn disrupts nuclear integrity, resulting in increased genotoxicity and decreased nuclear function (Fig 6).

Nuclear p-α-syn Sensitizes Cells to Nuclear Toxin Insult

Lasty, we examined whether decreased nuclear integrity affected susceptibility to nuclear insult and subsequent cell death. Neuro 2a cells were treated with increasing concentrations of doxorubicin, a DNA intercalator that inhibits topoisomerase II (Anders et al., 2013; Fornari et al., 1994; Pommier et al., 2010), for 24 hours and cell viability was subsequently recorded. Viability after 24 hours of doxorubicin treatment at 0.5 μM and less was significantly lower in cells with nuclear pathological α-syn (Fig 5C) ($p=0.0106$, Mann-Whitney test, $U=12$). This suggests the presence of nuclear α-syn sensitizes the cell to environmental insults. Collectively, these data have led to a working model that nuclear α-syn disturbs nuclear morphology and function (Fig 6).

Materials and Methods

<u>α-Syn Monomer Production:</u> Glycerol stocks of BLD21 E.Coli cells transfected with PRK172-α-synuclein plasmid (kind gift of Dr. Michael Goedert) were removed from storage and was transferred into a starter flask containing Terrific Broth (VWR) supplemented with 100 μg/mL ampicillin (VWR) and shaken overnight at 37 °C. The next day, starter culture was transferred to large culture flasks and incubated further until OD_{600}= 0.8, at

which point synuclein expression was induced with IPTG for 3 hours. Cell pellets were collected, lysed through sonication, boiled, and then centrifuged. The supernatant was then dialyzed overnight in SnakeSkin Dialysis Tubing, 3.5 MWCO (ThermoFisher) with gentle stirring.

The dialyzed lysate was then loaded onto a HiPrep Q HP 16/10 anion exchange chromatography (AEC) column (Cytiva) and probable fractions determined by OD_{280} nm peaks on the chromatograph, were loaded on 4-20% precast Tris-Glycine gels (Bio-Rad). The loaded gels were run at 120V to completion, briefly washed, and subsequently stained with GelCode Blue (ThermoFisher). α-syn-positive fractions (Sup. Fig. 5) were dialyzed overnight as described above at 4°C. The following day, sample was subjected to size exclusion chromatography (SEC) via running on a HiLoad 16/600 Superdex 200pg SEC column (Cytiva). Probable fractions were selected and processed as above (Sup. Fig. 5), before concentration to 10 mg/mL via centrifugation in Ultra-15 centrifugal filters (Amicon). Concentrated α-syn was incubated on High-Capacity Endotoxin Removal Resin (Pierce) for 1 hour to remove trace endotoxin. The endotoxin-free monomeric synuclein was then stored at -80°C until PFF production.

PFF Production: PFF's were manufactured as previously described in literature (Patterson et al., 2019). Briefly, monomeric alpha-synuclein was thawed and centrifuged 10 minutes at 15,000 xg at 4 °C. Supernatant was removed and protein concentration was determined on spectrophotometer. The desired amount of sample was then diluted to 5 mg/mL and 500 µL aliquots were placed into low-binding microcentrifuge tubes (Eppendorf). Tubes were placed into a thermal mixer (VWR) inside a 37 °C oven and left to shake for 7 days at 1000 rpm. After shaking, the sample was briefly centrifuged, supernatant discarded, and pellet resuspended in half of the initial shaking volume of fibrilization buffer (50mM Tris-HCl, 150mM KCl, pH7.5). A small aliquot of PFF's was mixed at an equal ratio with 8M guanidinium chloride (GnCl) and absorbance was measured on a NanoDrop (ThermoFisher) spectrophotometer. Beers law was used to determine PFF concentration from absorbance and sample was diluted to 5 mg/mL for short term storage and/or subsequent sonication.

Sonication and Dynamic Light Scattering: PFF's were transferred to 50 µl microtubes (Covaris) and placed into the sample holder of a M220 Focused-ultrasonicator (Covaris). Sonication protocol was executed with the following parameters: peak incidence power of 50%, duty factor of 10%, 1 second treatment time, 200 cycles per burst, and 220 iterations. Temperature control was set to 12°C +/- 2°C.

Proper sonication was verified via dynamic light scattering (DLS) analysis. A sonicated PFF aliquot was diluted 1:4 with PBS and transferred to a micro-capillary (Bettersize) via capillary action. Capillaries were placed into a BeNano 180 Zeta Pro (Bettersize) machine and the sizing protocol was performed. The average target size of 50 nm was used as quality cutoff (Sup. Fig. 5), and sample > 10 nm above the cutoff were either rejected or re-sonicated to specification.

Surgery: Male C57BL/6J mice 10-14 weeks of ager were anesthetized with 1-3% isoflurane in an induction chamber, and then transferred to a nose cone of an RWD or Stoelting sterotax. Mice were given Meloxicam (15 mg/kg, s.c.) as a general preoperative analgesic, and Bupivacaine (0.2-0.3 mL at a dose of 5 mg/mL, S.C.) as a local analgesic at the site of incisions. Fur was removed from the incision site via shaving prior to stabilization in a stereotaxic apparatus. Mice remained under anesthesia with a constant 1-1.5% isoflurane at between 1-2 L/min flow. The surgical site was disinfected with 4% chlorhexidine solution and sterile saline solution using cotton-tipped applicators. Burr holes were drilled above bilateral target coordinates (AP: 0.2, ML: +/- 2.0, DV: -2.8 from dura matter) using an Micro-Drill (IDEAL Part No. 67-1204). A 10 µL micro-syringe (Hamilton 1701 RN) was used to inject 2 µL of PFF or control at a rate of 0.5 µL/min/site. Following the injection, the needle was left in place for 5 minutes to allow for absorption before being slowly withdrawn. The surgical site was sutured using nylon 18"/45 cm surgical sutures and fixed in place using biocompatible glue (Vetbond) directly on the sutures. Mice were given 1 mL of saline at the end of the surgery to stave off dehydration, and were monitored postoperatively for two days after surgery, during which Meloxicam was given daily (15 mg/kg, S.C.).

Tissue Processing: At the desired time points post PFF injection, mice were anesthetized with isoflurane and transcardially perfused with ice-cold PBS followed by 4% paraformaldehyde. Brains were carefully extracted from the skull and post-fixed in 4% PFA for 24 hours before short-term storage in PBS with 0.05% sodium azide.

Whole brain tissue was mounted and processed on a Lieca Vibratome 1200S, calibrated to 18° clearance angle in ice-cold PBS. Slices under 100 µm were obtained and stored in 24-well plates in PBS with 0.05% sodium azide at 4°C until downstream use.

Cell Culture: Neuronal 2a cells were cultured in 6- well plates in DMEM medium supplemented with 5% FBS and 1x GlutaMAX (Gibco). Cells were housed in a 37°C humidified incubator with 5% CO_2 and ongoing cultures were subjected to media changes every 48 hours. At 80% confluency cells were dissociated with StemPro Accutase (Gibco) and passaged at a 1:4 ratio into new 6-well plates.

To create a population of cells with α-syn pathology, we subjected cells to incubation with α-syn PFF's. First, 5 mg/mL aliquots of PFF's were thawed and sonicated as described above. Next, PFF's were diluted 1 to 3:5 and mixed with BioPORTER QuickEase Protein Delivery Reagent (Millipore Sigma) for 5 minutes. The BioPORTER & PFF mixture was subsequently diluted up to 1.5 mL in serum free media. A single well of a 6-well dish was briefly washed 2x with serum free media and then incubated with the PFF/BioPORTER for 4 hours. Control wells were also subjected to serum free conditions. After 4 hours, the PFF media was aspirated, and cells were placed in normal growth medium. PFF-subjected cells were cultured separately and were incubated with PFF's as described each passage thereafter up to 6 total PFF incubations.

Immunofluorescence: All immunofluorescence labeling of tissue was performed in 24-well plates. Slices were briefly washed with PBS before 2 hours incubation in blocking/permeabilization buffer (5% normal donkey serum, 0.1% triton x-100) at room temperature with light shaking. Free-floating slices were next transferred into wells with primary antibody for overnight incubation at 4°C with gentle shaking. The next morning, tissue was washed 3x with PBS and stained with secondary antibody for 1 hour at room temperature. All antibodies and their dilutions are listed in Table 1. Mouse antibodies were diluted in mouse-on-mouse (M.O.M) diluent buffer (Vector laboratories) for labeling of murine tissue. All other antibodies were diluted in blocking/permeabilization buffer for murine and human tissue. After secondary labeling, samples were subsequently washed 3x with PBS, incubated in PBS with DAPI for 5 minutes, and washed 2x more times with PBS before imaging. Labeled slices were stored at 4°C in PBS .05% sodium azide.

Cell culture immunofluorescence was performed as above except Neuro 2a cells were plated into 8-well chamber slides (Cellvis) coated with Matrigel (Corning) for antibody labeling and imaging. For SYTO RNASelect labeling, the manufactures (Invitrogen) instructions were followed. Briefly, 500 nM solution was prepared in serum free media, incubated with cells for 20 minutes in a cell culture incubator. Cells were then post fixed in methanol at -20°C for 10 minutes, washed, and stored in PBS for imaging.

Western Blot Analysis: Neuro 2a cells were counted, centrifuged, and pellets were resuspended in 2x Lamelli sample buffer (Bio-Rad), briefly sonicated at 70% amplitude with a probe tip sonicator, heated for 10 minutes, and loaded onto 4-20% gradient SDS-PAGE gel. Gels were run at 120V to completion and transferred to PVDF membranes overnight at 20V and 4°C. Membranes were then briefly washed in PBS with 0.1% tween 20 (PBS-T) before blocking in 5% milk in PBS-T for 2 hours. Membranes were then incubated in primary antibodies overnight at 4°C with gentle shaking. The following morning, membranes were washed 3x with PBS-T and then incubated with fluorescent secondary antibodies for 1 hour. All antibodies used for biochemical analysis are listed in Table 1. After 3 final PBS-T washes, fluorescent signal in the 800 nm channel was captured on a Licor Odyssey XF imager. Fluorescent signal was quantified in Image studios software (LICORbio).

Spinning Disc Confocal Microscopy: Tissue slices were transferred to a glass bottom dish (MATTEK) with # 0.15 cover glass for imaging. The correction collars on 60x water immersion objective (Nikon) were set to 0.17 and water was applied to objectives before and during imaging sessions. For SoRa super resolution imaging, 4x magnification lens and 16-bit sensitive image acquisition settings were used. Images were acquired with 0.3 µm step size throughout the entire z-span of the cell(s) of interest. Diffraction-limited 60x objective images were acquired with 1x magnification. Saturation filters were enabled during imaging. Secondary antibody only controls were used to help determine acquisition settings and identify off target signal (Sup. Fig. 6). All acquisition for quantitative analysis was performed with identical settings between groups.

Three of the Lewy aggregates in human tissue were imaged on a Nikon CSU-W1 Spinning Disc, with Gataca super resolution modules and 100x silicon immersion lens. This system achieves similar resolution to SoRa super resolution imaging and our conservative "cutoff" resolution parameters were deemed appropriate for these images as well.

IMARIS Image analysis: All images were imported into IMARIS software (Oxford Instruments) for analysis and deconvolved with 50 µm pinhole size and water immersion settings selected. Images captured with 10x magnification air objectives had the air immersion setting selected. After deconvolution, the surfaces' function was used to create physical structures for nuclear lamina, DNA, and pathological α-syn for various analysis. Surface creation from fluorescent signal enables analysis in higher detail (Sup. Fig. 3). 53BP1 puncta were analyzed with spots function within IMARIS.

Discussion:

The nuclear localization of α-syn has remained controversial despite numerous reports of α-syn in the nuclei of various animal and cellular models both in pathogenic states and normal physiology (Goers et al., 2003; Liu et al., 2011; Maroteaux et al., 1988; McLean et al., 2000; Mori et al., 2002; Pinho et al., 2019; Schaser et al., 2019; Yu et al., 2007). Lack of nuclear characterization and off target nuclear staining associated with early α-syn antibodies may have contributed to this controversy (Huang et al., 2011; Koss et al., 2022). Studies have also forced nuclear localization of α-syn via adding a nuclear localization sequence and observed downstream detrimental nuclear function due to increased nuclear α-syn (T. Du et al., 2024; Pinho et al., 2019), suggesting α-syn is a critical regulator of nuclear function. Recently, pathological α-syn has been suggested in postmortem LBD tissue (Koss et al., 2022), raising questions as to potential pathological nuclear function and the downstream impact of nuclear p-α-syn. Using quantitative super resolution imaging, we rigorously report robust nuclear p-α-syn aggregates in our synucleinopathy mouse model, cell culture model, and postmortem human tissue. This nuclear localization is associated with functional and morphological nuclear abnormalities that raise a number of implications for future therapeutic avenues as well as pathogenesis of disease.

The abnormal nuclear morphological phenotypes we observed in synucleinopathy tissue from human and mouse closely resembles the morphological abnormalities observed in laminopathies, a group of disorders resulting from mutations in the *LMNA* and *LMNB* genes that encode the nuclear lamina proteins Lamin A/C and Lamin B respectively (Bonne et al., 1999; Worman, 2012). Laminopathies are associated with abnormal nuclei morphology and loss of nuclear integrity (Rankin & Ellard, 2006; Worman, 2012). We observed increased abnormal nuclei morphology in both murine and human synucleinopathy tissue, suggesting a common phenotype between synucleinopathies and laminopathies (Fig. 2F, 3).

Consistent with reports of α-syn induced nuclear damage in other synucleinopathy models and brain regions (Milanese et al., 2018; Szegö et al., 2022), we report for the first time, to our knowledge, that cortical neurons *in vivo* and cultured Neuro 2a cells post α-syn corruption by PFFs have increased 53BP1 nuclear localization (Fig 4A). 53BP1 is associated with a specific form of DNA damage that is closely associated with physical stress places on the nucleus (Isermann & Lammerding, 2017; Shah et al., 2021), correlating morphological changes in nuclear morphology to genotoxicity. Laminopathies are also associated with increased DNA damage and genotoxic markers (Earle et al., 2020; Gonzalo, 2014), drawing further similarity between laminopathies and synucleinopathies described in our models. Our data directly suggests that nuclear localization of pathological α-syn causes physical damage to the nuclear envelope, resulting in morphological changes associated with impaired function (Fig. 6).

Our data further shows impaired nuclear function as a result of the organelle damage described above. First, we observed apparent functional deficits in our cell culture model by labeling cells with an RNA specific dye. Synucleinopathy cells were found to contain significantly less cytoplasmic volume of RNA staining compared to controls (Fig 5A). Impaired mRNA export has been found to result from TAR DNA binding protein-43 (TDP-43) neuronal aggregation and is hypothesized to occur in other neuronal aggregation disorders (Woerner et al., 2016). Impaired protein export (Chen et al., 2020) has also been reported in pathogenic SCNA models. Our RNA labeling experiment suggests that RNA export is impaired in cells with α-syn pathology due to lack of cytoplasmic staining. Future studies will aim to elucidate the mechanistic impact of nuclear p-a-syn pathology on *Nxf1*

dependent export of mRNA (Viphakone et al., 2012), Exportin-t dependent export of tRNA (Kutay et al., 1998) and CRM1-dependent rRNA export (Bai et al., 2013).

Additional nuclear dysfunction was implicated via analysis of nuclear envelope repair pathways, that we investigated due to initial findings of envelope disfigurement and ruptures in nuclear lamina (Fig 3A). The endosomal sorting complex required for transport III complex (ESCRT-III) is well characterized in envelope repair (Raab et al., 2016; Willan et al., 2019). Within the envelope repair pathway (Fig 5B), LEMD2 localizes to envelope damage and recruits ESCRT-III component CHMP7, that subsequently recruits other ESCRT-III proteins (Gu et al., 2017). We interpret the observed increased LEMD2 expression but decreased CHMP7 expression as a likely increase in nuclear envelope damage but impaired ESCRT-III mediated repair. Future studies will aim to fully characterize the impact of nuclear p-α-syn on envelope repair mechanisms.

Finally, we investigated the impact of p-α-syn induced nuclear deficits on cell survival. Both in cell culture and rodent synucleinopathy models, accumulation of p-α-syn into aggregates was not directly associated with cell death. Therefore, we examined whether p-α-syn sensitizes cells to environment toxin induced cell death. Utilizing the nuclear damaging reagent doxorubicin, which alone has previously been shown to increase α-syn aggregation (Garg & Sinha, 2022) , we showed that cells with p-α-syn demonstrated decreased viability compared to control cells in response to low doxorubicin concentrations (Fig 5C) (Inoue et al., 2014). This is of interest, as increasing reports of environmental factors, such as pesticide exposure, increase synuclein aggregation and risk for developing synucleinopathies (Manning-Bog et al., 2002; S. S. Nielsen et al., 2015; Norris et al., 2007). This may give further support for a “two-hit” component in which genetic pre-disposition to α-syn aggregation, or accumulation of p-α-syn for other reasons, in combination with environmental stressors leads to or exacerbates diseases (Srivastava et al., 2020). We predict that nuclear damage induced by p-α-syn aggregation sensitizes neurons bearing aggregates to environmental insults, and that targeting nuclear based dysfunction caused by p-α-syn may be a novel mechanism by which to prevent cell death in synucleinopathies.

Cumulatively, our data demonstrates the presence of nuclear pathological α-syn at super resolution detail and reveals atypical downstream nuclear phenotypes resulting from this disease associated localization. The prevalence of the nuclear p-α-syn phenotype, observed impact on nuclear integrity, and functional impairment of the organelle, altogether suggest a relatively unexplored role for p-α-syn to disease etiology and cellular dysfunction in synucleinopathies. Additional mechanistic characterization of how p-α-syn localizes to the nucleus is necessary, and the full repercussions of nuclear p-α-syn are just beginning to be elucidated. Lastly, as different neuroanatomical regions respond uniquely to nuclear insults (Alhowail et al., 2021; J. Du et al., 2021; Lopes et al., 2008; Moruno-Manchon et al., 2018), we predict α-syn induced nuclear stress will impact various brain regions differently, and understanding disease signaling within and between brain regions may provide mechanistic insight into synucleinopathies and cell type selective vulnerability.

Acknowledgments

We would like to thank the laboratory of Dr. Jonathan Bird for providing access and technical assistance with Nikon CSU-W1 Spinning Disc with Gataca super resolution modules. We would also like to thank Bird laboratory member James Heiding’s, for expert liquid chromatography technical support. Thank you to the center for translational research in neurodegenerative disease (CTRND) for access to and maintenance of Nikon SORA super resolution microscope and cell culture facilities. Thank you to Dr. Michael Goedert for gifting us the alpha-synuclein plasmid. We sincerely thank the patients and families for the generous donation of human tissue used in this study. Additionally, we would like to thank the Harry T. Mangurian Foundation, Michael J. Fox Foundation 023031, National Institutes of health and National Institute of Neurological Disorders and Stroke R01NS11087 to MSM for funding this work. The UF HBTB is supported by the McKnight Brain Institute, the Center for Translational Research in Neurodegenerative Diseases at the University of Florida, and NIH grant P30AG066506. S.P. is the Charlotte and Howard Zimmerman Rising Star Professor with the Norman Fixel Institute for Neurological Diseases.

References

Aebi, U., Cohn, J., Buhle, L., & Gerace, L. (1986). The nuclear lamina is a meshwork of intermediate-type filaments. *Nature*, *323*(6088), 560–564.

Alhowail, A. H., Pinky, P. D., Eggert, M., Bloemer, J., Woodie, L. N., Buabeid, M. A., Bhattacharya, S., Jasper, S. L., Bhattacharya, D., & Dhanasekaran, M. (2021). Doxorubicin induces dysregulation of AMPA receptor and impairs hippocampal synaptic plasticity leading to learning and memory deficits. *Heliyon*, *7*(7).

Anders, C. K., Adamo, B., Karginova, O., Deal, A. M., Rawal, S., Darr, D., Schorzman, A., Santos, C., Bash, R., & Kafri, T. (2013). Pharmacokinetics and efficacy of PEGylated liposomal doxorubicin in an intracranial model of breast cancer. *PloS One*, *8*(5), e61359.

Anderson, J. P., Walker, D. E., Goldstein, J. M., De Laat, R., Banducci, K., Caccavello, R. J., Barbour, R., Huang, J., Kling, K., & Lee, M. (2006). Phosphorylation of Ser-129 is the dominant pathological modification of α-synuclein in familial and sporadic Lewy body disease. *Journal of Biological Chemistry*, *281*(40), 29739–29752.

Badonic, T., Frumkina, L. J., Jakovleva, N. I., & Hornáková, A. (1992). Ultrastructural changes of neurons in dependence on the death cause in human brain. *Functional and Developmental Morphology*, *2*(4), 231–234.

Bai, B., Moore, H. M., & Laiho, M. (2013). CRM1 and its ribosome export adaptor NMD3 localize to the nucleolus and affect rRNA synthesis. *Nucleus*, *4*(4), 315–325.

Blair, J. A., Wang, C., Hernandez, D., Siedlak, S. L., Rodgers, M. S., Achar, R. K., Fahmy, L. M., Torres, S. L., Petersen, R. B., & Zhu, X. (2016). Correction: Individual Case Analysis of Postmortem Interval Time on Brain Tissue Preservation. *Plos One*, *11*(6), e0157209.

Bonne, G., Barletta, M. R. Di, Varnous, S., Bécane, H.-M., Hammouda, E.-H., Merlini, L., Muntoni, F., Greenberg, C. R., Gary, F., & Urtizberea, J.-A. (1999). Mutations in the gene encoding lamin A/C cause autosomal dominant Emery-Dreifuss muscular dystrophy. *Nature Genetics*, *21*(3), 285–288.

Burré, J. (2015). The synaptic function of α-synuclein. *Journal of Parkinson's Disease*, *5*(4), 699–713.

Chen, V., Moncalvo, M., Tringali, D., Tagliafierro, L., Shriskanda, A., Ilich, E., Dong, W., Kantor, B., & Chiba-Falek, O. (2020). The mechanistic role of alpha-synuclein in the nucleus: impaired nuclear function caused by familial Parkinson's disease SNCA mutations. *Human Molecular Genetics*, *29*(18), 3107–3121.

Du, J., Zhang, A., Li, J., Liu, X., Wu, S., Wang, B., Wang, Y., & Jia, H. (2021). Doxorubicin-induced cognitive impairment: the mechanistic insights. *Frontiers in Oncology*, *11*, 673340.

Du, T., Li, G., Zong, Q., Luo, H., Pan, Y., & Ma, K. (2024). Nuclear alpha-synuclein accelerates cell senescence and neurodegeneration. *Immunity & Ageing*, *21*(1), 47.

Earle, A. J., Kirby, T. J., Fedorchak, G. R., Isermann, P., Patel, J., Iruvanti, S., Moore, S. A., Bonne, G., Wallrath, L. L., & Lammerding, J. (2020). Mutant lamins cause nuclear envelope rupture and DNA damage in skeletal muscle cells. *Nature Materials*, *19*(4), 464–473.

Fornari, F. A., Randolph, J. K., Yalowich, J. C., Ritke, M. K., & Gewirtz, D. A. (1994). Interference by doxorubicin with DNA unwinding in MCF-7 breast tumor cells. *Molecular Pharmacology*, *45*(4), 649–656.

Fujiwara, H., Hasegawa, M., Dohmae, N., Kawashima, A., Masliah, E., Goldberg, M. S., Shen, J., Takio, K., & Iwatsubo, T. (2002). α-Synuclein is phosphorylated in synucleinopathy lesions. *Nature Cell Biology*, *4*(2), 160–164.

Garg, A., & Sinha, S. (2022). Doxorubicin induced aggregation of α-synuclein: insights into the mechanism of drug induced Parkinsonism. *Colloids and Surfaces B: Biointerfaces*, *212*, 112371.

Goers, J., Manning-Bog, A. B., McCormack, A. L., Millett, I. S., Doniach, S., Di Monte, D. A., Uversky, V. N., & Fink, A. L. (2003). Nuclear localization of α-synuclein and its interaction with histones. *Biochemistry*, *42*(28), 8465–8471.

Gonzalo, S. (2014). DNA damage and lamins. *Cancer Biology and the Nuclear Envelope: Recent Advances May Elucidate Past Paradoxes*, 377–399.

Gu, M., LaJoie, D., Chen, O. S., Von Appen, A., Ladinsky, M. S., Redd, M. J., Nikolova, L., Bjorkman, P. J., Sundquist, W. I., & Ullman, K. S. (2017). LEM2 recruits CHMP7 for ESCRT-mediated nuclear envelope closure in fission yeast and human cells. *Proceedings of the National Academy of Sciences*, *114*(11), E2166–E2175.

Huang, Z., Xu, Z., Wu, Y., & Zhou, Y. (2011). Determining nuclear localization of alpha-synuclein in mouse brains. *Neuroscience*, *199*, 318–332.

Inoue, S., Setoyama, Y., & Odaka, A. (2014). Doxorubicin treatment induces tumor cell death followed by immunomodulation in a murine neuroblastoma model. *Experimental and Therapeutic Medicine*, *7*(3), 703–708.

Isermann, P., & Lammerding, J. (2017). Consequences of a tight squeeze: Nuclear envelope rupture and repair. *Nucleus*, *8*(3), 268–274.

Jamali, T., Jamali, Y., Mehrbod, M., & Mofrad, M. R. K. (2011). Nuclear pore complex: biochemistry and biophysics of nucleocytoplasmic transport in health and disease. *International Review of Cell and Molecular Biology*, *287*, 233–286.

Jo, E., McLaurin, J., Yip, C. M., George-Hyslop, P. S., & Fraser, P. E. (2000). α-Synuclein membrane interactions and lipid specificity. *Journal of Biological Chemistry*, *275*(44), 34328–34334.

Koss, D. J., Erskine, D., Porter, A., Palmoski, P., Menon, H., Todd, O. G. J., Leite, M., Attems, J., & Outeiro, T. F. (2022). Nuclear alpha-synuclein is present in the human brain and is modified in dementia with Lewy bodies. *Acta Neuropathologica Communications*, *10*(1), 98.

Kutay, U., Lipowsky, G., Izaurralde, E., Bischoff, F. R., Schwarzmaier, P., Hartmann, E., & Görlich, D. (1998). Identification of a tRNA-specific nuclear export receptor. *Molecular Cell*, *1*(3), 359–369.

Lewy, F. H. (1912). Paralysis agitans. I. Pathologische anatomie. *Handbuch Der Neurologie*, *3*, 920–958.

Liu, X., Lee, Y. J., Liou, L.-C., Ren, Q., Zhang, Z., Wang, S., & Witt, S. N. (2011). Alpha-synuclein functions in the nucleus to protect against hydroxyurea-induced replication stress in yeast. *Human Molecular Genetics*, *20*(17), 3401–3414.

Lopes, M. Â., Meisel, A., Dirnagl, U., Carvalho, F. D., & de Lourdes Bastos, M. (2008). Doxorubicin induces biphasic neurotoxicity to rat cortical neurons. *Neurotoxicology*, *29*(2), 286–293.

Man, W. K., Tahirbegi, B., Vrettas, M. D., Preet, S., Ying, L., Vendruscolo, M., De Simone, A., & Fusco, G. (2021). The docking of synaptic vesicles on the presynaptic membrane induced by α-synuclein is modulated by lipid composition. *Nature Communications*, *12*(1), 927.

Manning-Bog, A. B., McCormack, A. L., Li, J., Uversky, V. N., Fink, A. L., & Di Monte, D. A. (2002). The herbicide paraquat causes up-regulation and aggregation of α-synuclein in mice: paraquat and α-synuclein. *Journal of Biological Chemistry*, *277*(3), 1641–1644.

Maroteaux, L., Campanelli, J. T., & Scheller, R. H. (1988). Synuclein: a neuron-specific protein localized to the nucleus and presynaptic nerve terminal. *Journal of Neuroscience*, *8*(8), 2804–2815.

McLean, P. J., Ribich, S., & Hyman, B. T. (2000a). Subcellular localization of α-synuclein in primary neuronal cultures: effect of missense mutations. *Advances in Research on Neurodegeneration: Volume 7*, 53–63.

McLean, P. J., Ribich, S., & Hyman, B. T. (2000b). Subcellular localization of α-synuclein in primary neuronal cultures: effect of missense mutations. *Advances in Research on Neurodegeneration: Volume 7*, 53–63.

Milanese, C., Cerri, S., Ulusoy, A., Gornati, S. V, Plat, A., Gabriels, S., Blandini, F., Di Monte, D. A., Hoeijmakers, J. H., & Mastroberardino, P. G. (2018). Activation of the DNA damage response in vivo in synucleinopathy models of Parkinson's disease. *Cell Death & Disease*, *9*(8), 818.

Mori, F., Tanji, K., Yoshimoto, M., Takahashi, H., & Wakabayashi, K. (2002a). Immunohistochemical comparison of α-and β-synuclein in adult rat central nervous system. *Brain Research*, *941*(1–2), 118–126.

Mori, F., Tanji, K., Yoshimoto, M., Takahashi, H., & Wakabayashi, K. (2002b). Immunohistochemical comparison of α-and β-synuclein in adult rat central nervous system. *Brain Research*, *941*(1–2), 118–126.

Moruno-Manchon, J. F., Uzor, N.-E., Kesler, S. R., Wefel, J. S., Townley, D. M., Nagaraja, A. S., Pradeep, S., Mangala, L. S., Sood, A. K., & Tsvetkov, A. S. (2018). Peroxisomes contribute to oxidative stress in neurons during doxorubicin-based chemotherapy. *Molecular and Cellular Neuroscience*, *86*, 65–71.

Nielsen, M. S., Vorum, H., Lindersson, E., & Jensen, P. H. (2001). Ca2+ binding to α-synuclein regulates ligand binding and oligomerization. *Journal of Biological Chemistry*, *276*(25), 22680–22684.

Nielsen, S. S., Checkoway, H., Zhang, J., Hofmann, J. N., Keifer, M. C., Paulsen, M., Farin, F. M., Cook, T. J., & Simpson, C. D. (2015). Blood α-synuclein in agricultural pesticide handlers in central Washington State. *Environmental Research*, *136*, 75–81.

Norris, E. H., Uryu, K., Leight, S., Giasson, B. I., Trojanowski, J. Q., & Lee, V. M.-Y. (2007). Pesticide exposure exacerbates α-synucleinopathy in an A53T transgenic mouse model. *The American Journal of Pathology*, *170*(2), 658–666.

Okochi, M., Walter, J., Koyama, A., Nakajo, S., Baba, M., Iwatsubo, T., Meijer, L., Kahle, P. J., & Haass, C. (2000). Constitutive phosphorylation of the Parkinson's disease associated α-synuclein. *Journal of Biological Chemistry*, *275*(1), 390–397.

Pan, Y., Zong, Q., Li, G., Wu, Z., Du, T., Zhang, Y., Huang, Z., & Ma, K. (2023). Nuclear localization of alpha-synuclein induces anxiety-like behavior in mice by decreasing hippocampal neurogenesis and pathologically affecting amygdala circuits. *Neuroscience Letters*, *816*, 137490.

Parra-Rivas, L. A., Madhivanan, K., Aulston, B. D., Wang, L., Prakashchand, D. D., Boyer, N. P., Saia-Cereda, V. M., Branes-Guerrero, K., Pizzo, D. P., & Bagchi, P. (2023). Serine-129 phosphorylation of α-synuclein is an activity-dependent trigger for physiologic protein-protein interactions and synaptic function. *Neuron*, *111*(24), 4006–4023.

Patterson, J. R., Polinski, N. K., Duffy, M. F., Kemp, C. J., Luk, K. C., Volpicelli-Daley, L. A., Kanaan, N. M., & Sortwell, C. E. (2019). Generation of alpha-synuclein preformed fibrils from monomers and use in vivo. *Journal of Visualized Experiments: JoVE*, *148*, 10–3791.

Pinho, R., Paiva, I., Jerčić, K. G., Fonseca-Ornelas, L., Gerhardt, E., Fahlbusch, C., Garcia-Esparcia, P., Kerimoglu, C., Pavlou, M. A. S., & Villar-Piqué, A. (2019). Nuclear localization and phosphorylation modulate pathological effects of alpha-synuclein. *Human Molecular Genetics*, *28*(1), 31–50.

Pommier, Y., Leo, E., Zhang, H., & Marchand, C. (2010). DNA topoisomerases and their poisoning by anticancer and antibacterial drugs. *Chemistry & Biology*, *17*(5), 421–433.

Raab, M., Gentili, M., de Belly, H., Thiam, H.-R., Vargas, P., Jimenez, A. J., Lautenschlaeger, F., Voituriez, R., Lennon-Duménil, A.-M., & Manel, N. (2016). ESCRT III repairs nuclear envelope ruptures during cell migration to limit DNA damage and cell death. *Science*, *352*(6283), 359–362.

Rankin, J., & Ellard, S. (2006). The laminopathies: a clinical review. *Clinical Genetics*, *70*(4), 261–274.

Sang, J. C., Hidari, E., Meisl, G., Ranasinghe, R. T., Spillantini, M. G., & Klenerman, D. (2021). Super-resolution imaging reveals α-synuclein seeded aggregation in SH-SY5Y cells. *Communications Biology*, *4*(1), 613.

Schaser, A. J., Osterberg, V. R., Dent, S. E., Stackhouse, T. L., Wakeham, C. M., Boutros, S. W., Weston, L. J., Owen, N., Weissman, T. A., & Luna, E. (2019). Alpha-synuclein is a DNA binding protein that modulates DNA repair with implications for Lewy body disorders. *Scientific Reports*, *9*(1), 10919.

Shah, P., Hobson, C. M., Cheng, S., Colville, M. J., Paszek, M. J., Superfine, R., & Lammerding, J. (2021). Nuclear deformation causes DNA damage by increasing replication stress. *Current Biology*, *31*(4), 753–765.

Snead, D., & Eliezer, D. (2014). Alpha-synuclein function and dysfunction on cellular membranes. *Experimental Neurobiology*, *23*(4), 292.

Srivastava, T., Raj, R., & Dubey, A. (2020). *Fast kinetics of environmentally induced α-synuclein aggregation mediated by structural alteration in NAC region and result in structure dependent cytotoxicity. Sci Rep 10: 18412*.

Szegö, E. M., Van den Haute, C., Höfs, L., Baekelandt, V., Van der Perren, A., & Falkenburger, B. H. (2022). Rab7 reduces α-synuclein toxicity in rats and primary neurons. *Experimental Neurology*, *347*, 113900.

Viphakone, N., Hautbergue, G. M., Walsh, M., Chang, C.-T., Holland, A., Folco, E. G., Reed, R., & Wilson, S. A. (2012). TREX exposes the RNA-binding domain of Nxf1 to enable mRNA export. *Nature Communications*, *3*(1), 1006.

Wadell, H. (1932). Volume, shape, and roundness of rock particles. *The Journal of Geology*, *40*(5), 443–451.

Willan, J., Cleasby, A. J., Flores-Rodriguez, N., Stefani, F., Rinaldo, C., Pisciottani, A., Grant, E., Woodman, P., Bryant, H. E., & Ciani, B. (2019). ESCRT-III is necessary for the integrity of the nuclear envelope in micronuclei but is aberrant at ruptured micronuclear envelopes generating damage. *Oncogenesis*, *8*(5), 29.

Woerner, A. C., Frottin, F., Hornburg, D., Feng, L. R., Meissner, F., Patra, M., Tatzelt, J., Mann, M., Winklhofer, K. F., & Hartl, F. U. (2016). Cytoplasmic protein aggregates interfere with nucleocytoplasmic transport of protein and RNA. *Science*, *351*(6269), 173–176.

Worman, H. J. (2012). Nuclear lamins and laminopathies. *The Journal of Pathology*, *226*(2), 316–325.

Yu, S., Li, X., Liu, G., Han, J., Zhang, C., Li, Y., Xu, S., Liu, C., Gao, Y., & Yang, H. (2007). Extensive nuclear localization of α-synuclein in normal rat brain neurons revealed by a novel monoclonal antibody. *Neuroscience*, *145*(2), 539–555.

Microscopy	Western Blots	Cell Culture
Anti-Alpha-synuclein (phospho S129) antibody [EP1536Y] (Cat # ab51253)	CHMP7 Polyclonal antibody (Cat #16424-1-AP)	Gibco™ DMEM, high glucose (Cat # 11965118)
Anti-Lamin A + Lamin C antibody [4C11] (Cat #ab238303)	LEMD2 Polyclonal antibody (Cat # 29406-1-AP)	BioPORTER® QuikEase™ Protein Delivery Kit (BPQ24)
DAPI (4',6-diamidino-2-phenylindole, dihydrochloride) (Cat # PI62247)	53BP1 Antibody (Cat # 4937S)	Gibco™ GlutaMAX™ Supplement (Cat # 35050061)
Donkey Anti-Rabbit IgG (H+L), Highly Cross-Adsorbed, CF® Dye Conjugate 568 (Cat # 20803)	Anti-alpha Tubulin antibody [DM1A] - Loading Control (Cat # ab7291)	Nunc™ Cell-Culture Treated 6-well Dish (Cat #140675)
Donkey Anti-Mouse IgG (H+L), Highly Cross-Adsorbed (Min X Rat) CF® Dye Conjugate 660R (Cat # 20388)	IRDye® 800CW Goat anti-Mouse IgG Secondary Antibody (Cat # 926-32210)	StemPro™ Accutase™ Cell Dissociation Reagent (Cat # A1110501)
Normal Donkey Serum (Cat # 017-000-121)	IRDye® 800CW Goat anti-Rabbit IgG Secondary Antibody (Cat # 926-32211)	Gibco™ Fetal Bovine Serum (FBS) (Cat # A5670701)
PBS, Phosphate Buffered Saline, 10X Solution, Fisher BioReagents™ (Cat # BP39920)	Carnation Instant Nonfat Dry Milk (Cat # 12428935)	8 Well chambered cover Glass with #1.5 high performance cover glass (Cat # C8-1.5H-N)
Chicken Polyclonal Antibody to α-Synuclein (Cat #PCA-SNCA)	PBS, Phosphate Buffered Saline, 10X Solution, Fisher BioReagents™ (Cat # BP39920)	Doxorubicin hydrochloride (Cat # 44583)
53BP1 Antibody (Cat # 4937S)	TWEEN® 20 (Cat # P1379)	CellTiter-Glo® 2.0 Cell Viability Assay (Cat # G9241)
Triton™ X-100 (Cat # X100)	PVDF Transfer Membrane (Cat #88518)	SYTO® RNASelect™ Green Fluorescent Cell Stain (Cat # S32703)
Glass Bottom Imaging Dish (Cat # P50G-1.5-30-F)		
Mouse on Mouse (M.O.M.) Kit (Cat # BMK-2202)		

Table 1: Materials and Reagents: Microscopy (Left Column), Western Blots (Center Column), and Cell Culture (Right Column).

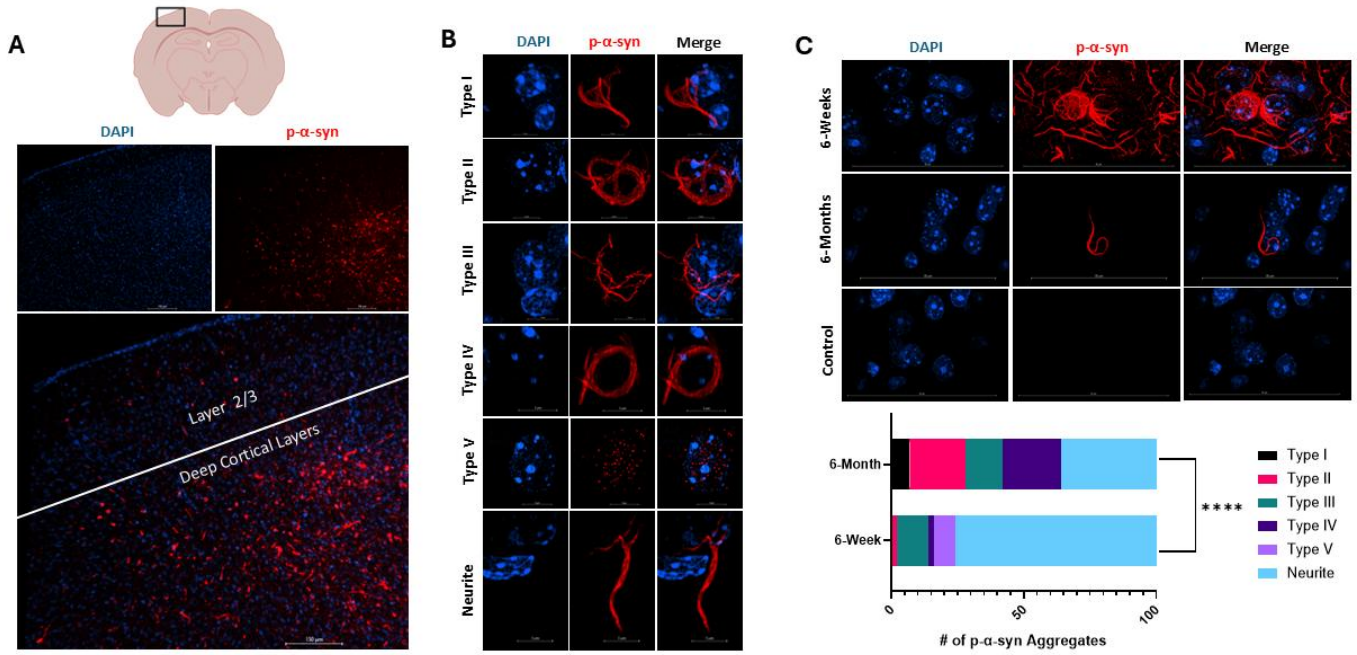

Figure 1: Synucleinopathy Mice Display Robust Cortical Lewy-like Pathology. A) Illustration depicting coronal slice of mouse brain tissue (Top), black box indicates example region of interest for imaging (Top). Representative micrograph of cortical Lewy-like Pathology at 10x magnification (Bottom). B) Murine cortical Lewy-like pathology assumes six predominant morphologies. C) Pathological α-syn aggregation dynamics over time. Micrographs of representative pathology at 6-week and 6-month timepoints post PFF injection (Top). Quantification of aggregate morphology at 6-weeks and 6-months post PFF injection (Bottom). Of 100 aggregates analyzed at 6-weeks post PFF injection, we found; 0 Type 1, 2 Type II, 12 Type III, 2 Type IV, 8 Type V, and 76 Neurites. Analysis of tissue harvested 6-months post PFF injection yielded; 7 Type 1, 21 Type II, 14 Type III, 22 Type IV, 0 Type V, and 36 Neurites. N= 3 mice, n=100 aggregates ($p<0.0001$, Fisher's Exact Test).

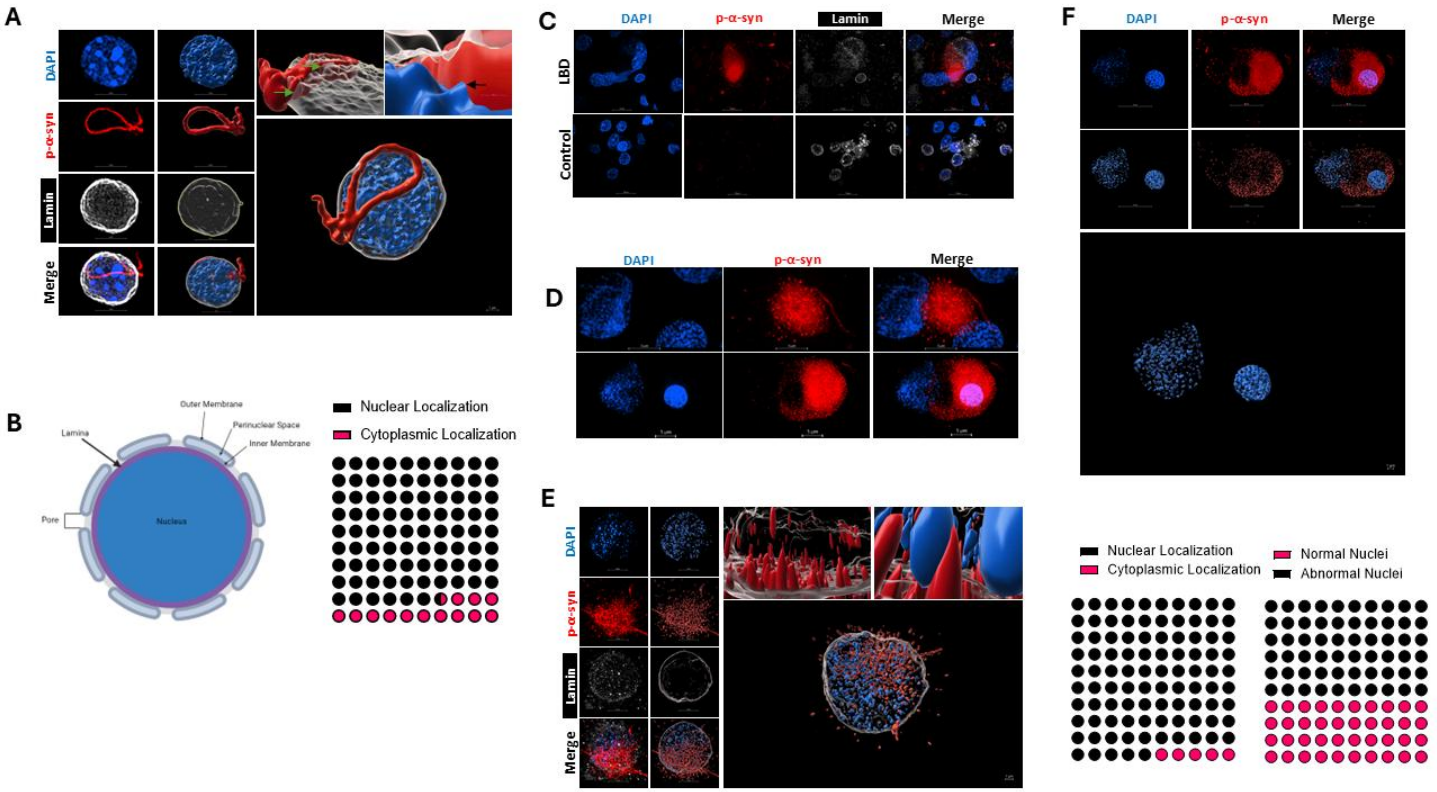

Figure 2: **Pathological α-Syn Localizes Within Nuclear Compartments. A)** Surface Renderings were created for each Nuclear structure of interest and p-α-syn (Left). 3D surface renderings of p-α-syn interacting with the nuclear lamina (Top, Right) and an inside view of cell nucleus interacting with p-α-syn (Top, Right). Green arrows indicate portions of the lamina where p-α-syn passes through the Lamin coating. Black arrow depicts colocalization of DAPI and p-α-syn. **B)** Schematic depicting rudimentary nuclear envelope anatomy (Left). Nuclear Lamina (depicted in purple) proteins were used as a boundary structure to classify localization of α-syn within the nucleus. Quantification of p-α-syn localized withing the nuclear lamina yielded 86.7% (95% CI 70.32-94.69%) of aggregates with nuclear localization. N=3 Mice, n= 30 cells ($p<0.0001$, Binomial test) **C)** Representative 60x SoRa field of view micrographs of human cingulate cortex tissue. Lewy Body Dementia (LBD) tissue (Top) and control tissue (Bottom). **D)** Lewy Pathology observed was punctate inclusions either with (Top) or without (Bottom) a fibril-like component. **E)** Lamin surfaces were generated for visualization purposes on high integrity nuclei. **F)** Nuclear localization was quantified by co-localization of p-α-syn with DAPI. Quantification of nuclear localization (Bottom, Left) revealed 95% (95% CI 76.39 to 99.74) of aggregates analyzed have nuclear localization ($p<0.0001$, Binomial test). N= 3 LBD Cingulate cortices, n= 20 aggregates. Of the nuclei these aggregates interacted with, 60% (95% CI 38.66 to 78.12) displayed aberrant morphology (Bottom, Right) ($p<0.0001$, Binomial test). N= 3 LBD Cingulate cortices, n= 20 aggregates.

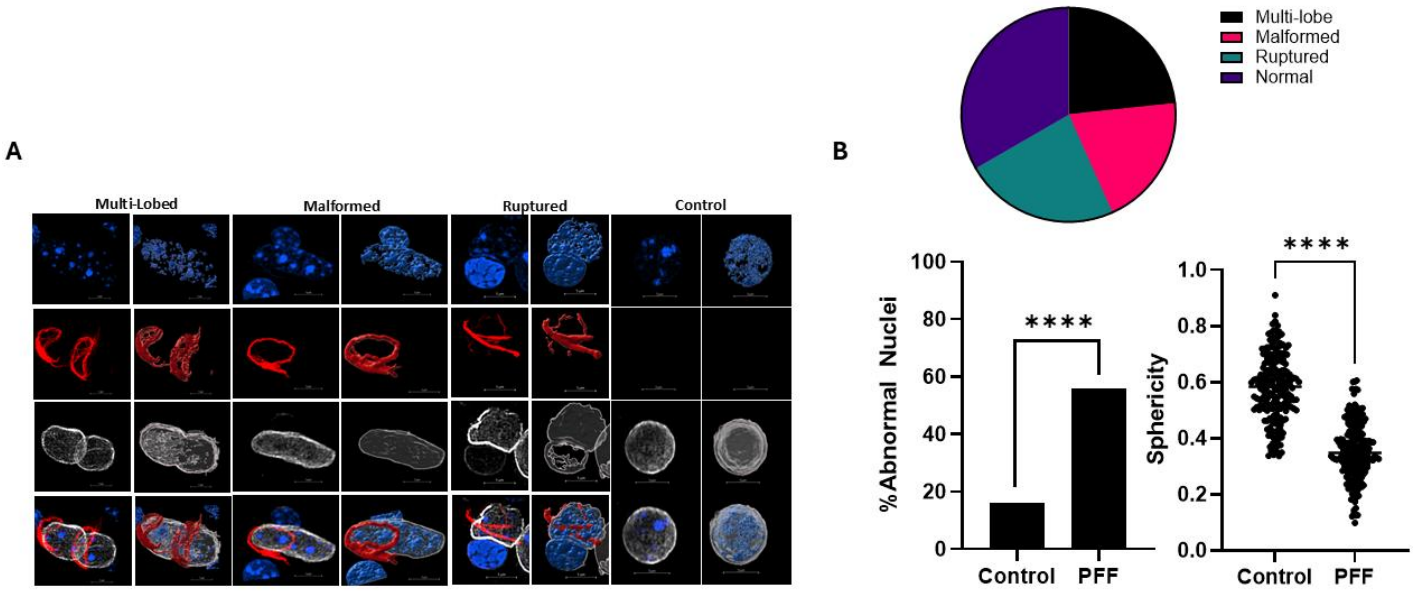

Figure 3: Nuclear p-α-Syn Induces Nuclear Abnormalities. A) Abnormal nuclei broadly fell into three categories; multi-lobed, malformed, and/or ruptured. Representative control nuclei shown (right column). N= 3 mice, n=50 nuclei. **B)** Quantification of figure 2A. Percent of abnormal cells in control and synucleinopathy tissue (Bottom, Left) in qualitative analysis revealed 56% (95% CI 42.31 to 68.84) of synucleinopathy nuclei were abnormal, significantly more than the 16% (95% CI 8.337 to 28.51) of abnormal control nuclei ($p<0.0001$, Chi-square value 17.36, df 1), N=3 Mice, n=50 nuclei. Distribution of abnormal nuclei classifications in cortical synucleinopathy tissue (Top) from the cells examined in Fig. 2B. SoRa super resolution image analysis yielded 66.7% (95% CI 48.78 to 80.77) of nuclei associated with p-α-syn aggregates were associated with abnormal nuclear morphology ($p<0.0001$, Binomial Test). Of the abnormal nuclei; 35% (95% CI 11.79-40.93) of nuclei were multi-lobed, 30% (95% CI 9.51-37.31) were malformed, and 35% (95% CI 11.79-40.93) appeared ruptured (Top). Sphericity(ψ) of cortical cell quantified in control and synucleinopathy tissue (Bottom, Right). Control tissue averaged ψ=0.5836 (95% CI 0.5678-0.5994) and PFF treated tissue averaged ψ=0.3550 (95% CI 0.3414-0.3687) N= 3 mice, n= 210 cells ($p <0.0001$, Unpaired-T test, t=21.60).

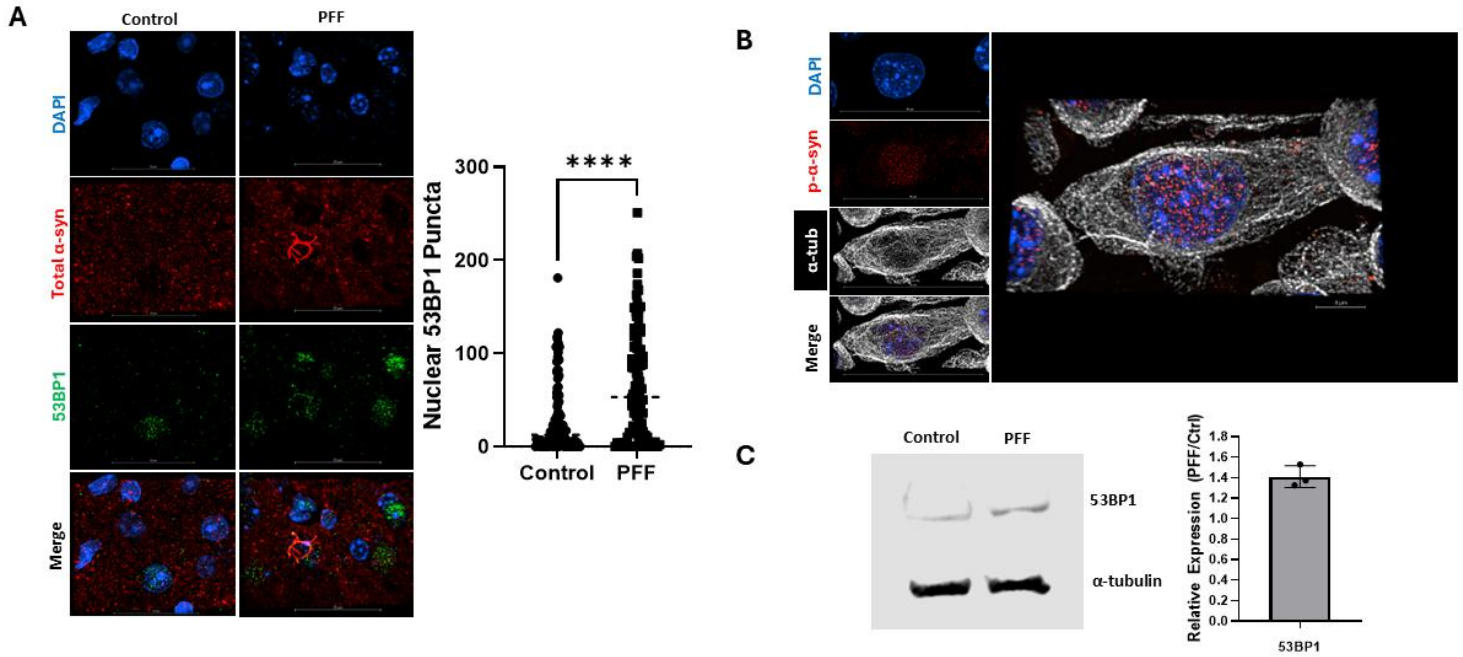

Figure 4: Synucleinopathy Models Have Increased Genotoxicity A) C57BL6 murine cortical cells display increased 53BP1 puncta compared to wild type tissue. Quantification (Right) yielded an average of 66.89 puncta (95% CI 54.89-78.89) per synucleinopathy cell while control cortical cells averaged 29.64 53BP1 puncta per cell (95% CI 22.10-37.18).N=3 mice, n=100 cells ($p<0.0001$, Unpaired-T test,$t=5.215$). **B)** PFF treated Neuro 2a cells accumulate pathological syn in nucleus. **C)** Nuclear accumulation of p-α-syn in Neuro 2a cells is associated with increased 53BP1 genotoxicity marker average 1.409x (95% CI 1.146- 1.673) times greater than control cells normalized to a value of 1. N=3 cell culture dishes ($p=0.0026$, Unpaired-T test, $t=6.678$).

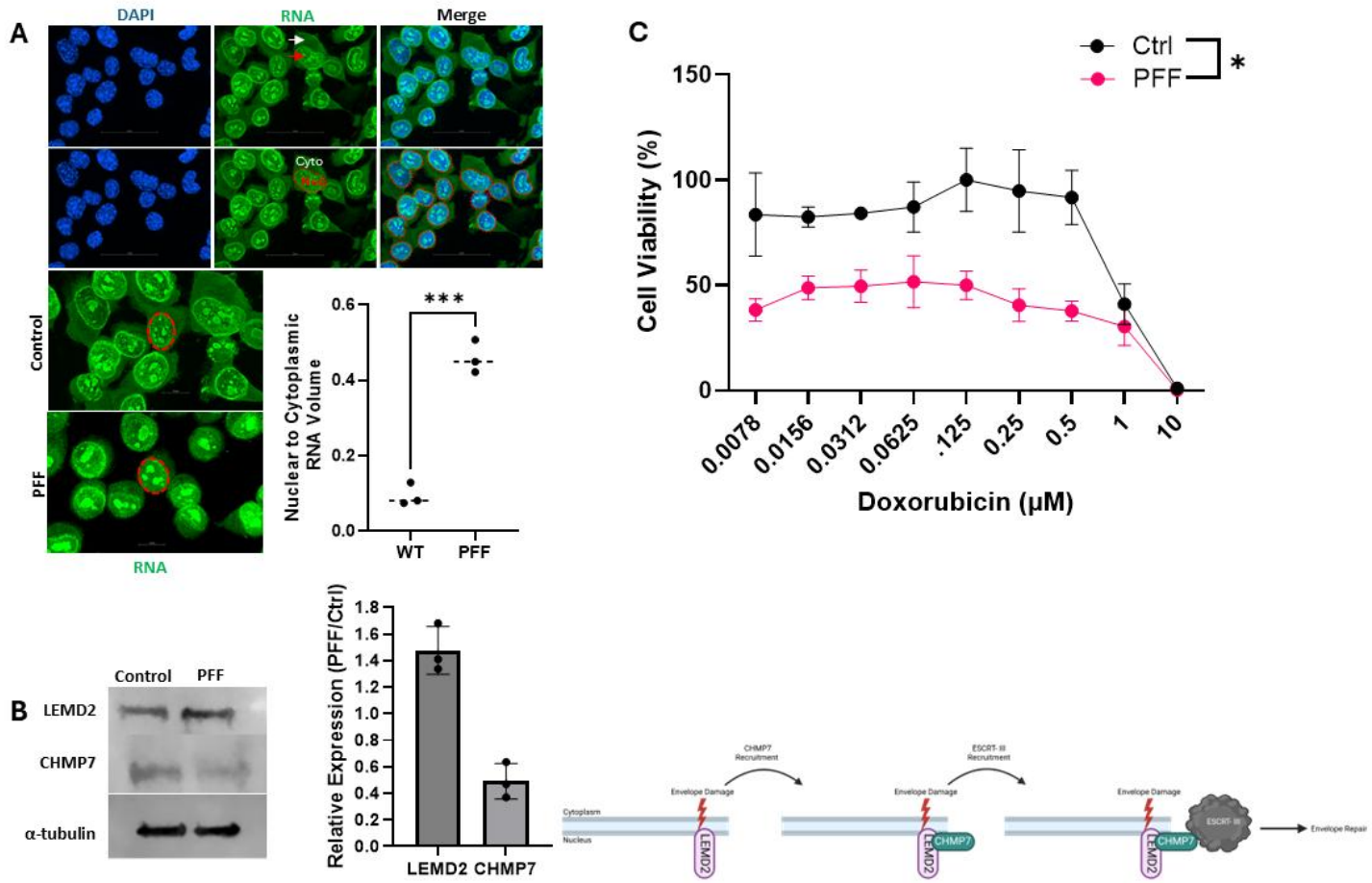

Figure 5: Pathological α-Syn Accumulation Results in Nuclear Deficits. A) RNASelect labeling of Neuro 2a cells clearly defines nucleoli (Red Arrow) and nuclear borders (red dotted line). All fluorescent signal outside of this border was considered cytoplasmic (White Arrow). Quantification of staining volume distribution between nucleus and cytoplasm (Bottom) in control and PFF treated cells yielded an of 0.4954 (95% CI 0.3508-0.5679) for synucleinopathy tissue, and 0.09499 (95% CI0.02112-0.1689) for control tissue. N=3 culture dishes, n >100 cells (p=0.0003, Unpaired-T test, t =11.94). **B)** Western blot analysis of envelope repair pathway proteins in control and synucleinopathy tissue. Alpha-tubulin (α-tubulin) loading control shown on bottom. Quantification of western blots (Middle). Synucleinopathy cells displayed a 1.476x increase in LEMD2 (p=0.0103, Unpaired-T test, t=4.568) and a 0.4910x (95% CI 0.8243- 0.1578) decrease in CHMP7 expression (p=0.00028, Unpaired-T test, t=6.572). Visual rendering of simplified ESCRT-III mediated envelope repair pathway (Right). **C)** Neuro 2a cells were treated with varying concentrations of Doxorubicin for 24 hours. Cell viability was recorded with Cell Titer Glo 2.0 reagent and normalized to untreated wells. (p=0.0106, Mann-Whitney test, U=12). N=3 culture dishes, n= 6 technical replicates.

A

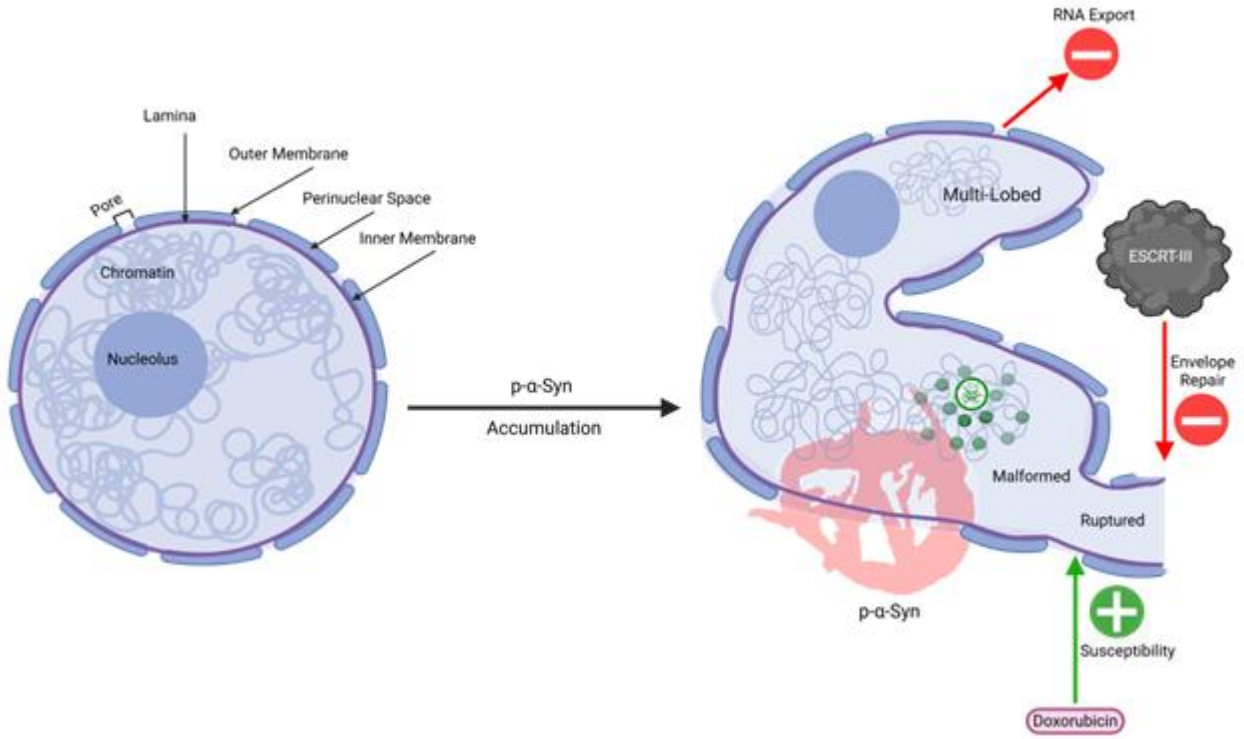

Fig. 6: Intranuclear p-α-Syn Compromises Integrity and Function of the Nucleus. A) Visual rendering of our working hypothesis on pathological α-syn nuclear localization and downstream consequences. Nuclear Localization of p-α-syn results in abnormal nuclear morphology, namely rupturing, malformation, and formation of multiple lobes. Abnormal morphology is correlated with an increase in 53BP1 genotoxicity (green puncta), decreased ESCRT-III component expression (which we predict decreased envelope repair as a result), aberrant RNA localization (which we predict is due to impaired RNA export), and increased sensitivity to environmental insult, namely doxorubicin.